Supporting Online Material for

Dynamic Analyses of *Drosophila* Gastrulation Provide Insights into Collective Cell Migration

Amy McMahon, Willy Supatto, Scott E. Fraser, Angelike Stathopoulos*

*To whom correspondence should be addressed. E-mail: angelike@caltech.edu

Published 5 December 2008, *Science* **322**, 1546 (2008)
DOI: 10.1126/science.1167094

This PDF file includes:

Other Supporting Online Material for this manuscript includes the following:
(available at www.sciencemag.org/cgi/content/full/322/5907/1546/DC1)

Supporting Online Materials:

I. Materials and Methods

II. Supplemental Figures

Figure S1. Coordinate systems used during imaging and analysis processes.

Figure S2. Virtual cross-sections and tracking data for H2A-GFP embryos in wild-type and *htl* mutant backgrounds.

Figure S3. Decomposition of movement, correlation data and ectoderm subtraction for *htl* mutant embryos.

Figure S4. Spreading consistency analysis: $\theta_{start}(\theta_{end})$ graphs.

Figure S5. Spreading consistency analysis: table of linear regression and main conclusions.

Figure S6. Wild-type and *klarschist* embryos show similar morphology in fixed sections.

Figure S7. Disrupting the spatial or temporal patterns of division in the mesoderm does not affect the spreading pattern.

III. Movies Legends

Movie S1: Two-photon excitation of ubiquitous H2A-GFP in early embryos.

Movie S2: Segmentation and tracking of mesoderm nuclei in wild-type embryos using Imaris software.

Movie S3: 3D tracks of mesoderm and ectoderm cells over time.

Movie S4: Visualization of cylindrical coordinate system.

Movie S5: Ectoderm subtraction in a wild-type embryo (simulation).

Movie S6: Ectoderm subtraction in a wild-type embryo (experimental data).

Movie S7: Wild-type data along radial and angular axes (theta color code).

Movie S8: Wild-type data along radial and angular axes (radial color code).

Movie S9: Segmentation and tracking of mesoderm nuclei in *htl* mutant.

Movie S10: *heartless* data along radial and angular axes (theta color code).

Movie S11: *heartless* data along radial and angular axes (radial color code).

IV. References

I. Materials and Methods

Fly Strains and Genetics

All crosses and strains were maintained at 25°C. The following lines were obtained from Bloomington: His2AV-GFP; *htl*^{AB42}/TM3; *klar*^{1}; Dr/TM3, P(Dfd-GMR-nvYFP)3, Sb^{1}. His2AV-GFP was recombined with *htl*^{AB42} and *klar*^{1} using conventional methods. His2AV-GFP, *klar*^{1}, *htl*^{AB42} flies were maintained over a Dfd-GMR-YFP balancer. Wild-type refers to *yw* mutants or His2AV-GFP in a *yw* background.

Fixation for Antibody staining

Embryos were dechorionated for 3 minutes in bleach and washed thoroughly with 0.1% Triton NaCl and distilled H_2O. Embryos were fixed in 50% Heptane, 4% Formaldehyde, 0.25M EGTA, and PBS for 20 minutes. Vitelline membranes were removed by vigorous shaking of embryos in Methanol.

Antibody staining and Sectioning of Embryos

Color substrate staining was performed using the VectaStain kits (Vector). Embryos were blocked in 1.5% goat serum in PBS for 30 minutes. Primary antibodies were added overnight at 4°T. Guinea pig anti-Twist antibody (kind gift of Mike Levine, UC Berkeley) was used at 1:300 and secondary antibodies from the kit were used at 1:200. Sectioning was performed according to previous methods (Leptin and Grimwalde, 1990). Embryos were embedded in Araldite (Electron Microscopy Sciences) and hardened overnight at 55°C. Embryos were sectioned in 7 micron slices and mounted on slides with 50% Araldite/50% Acetone. Sections were visualized using an Axioplan microscope (Carl Zeiss Inc.) and Nomarksi optics.

Fluorescent staining was achieved with mouse anti-Neurotactin (BP106, DSHB) and guinea pig anti-Twist antibodies, at dilutions of 1:10 and 1:300, respectively. Secondary antibodies were added as a 1:400 dilution of either anti-mouse 543 or anti-guinea pig 488 (Molecular Probes, Invitrogen). Embryos were mounted in 70% glycerol

and sectioned with a standard razor blade. Images were taken on a Zeiss LSM 310 upright confocal microscope (Carl Zeiss Inc.).

2PEF microscopy

Mesoderm spreading in *Drosophila* involves fast cell movements, up to 10 $\mu m.min^{-1}$ occurring during two hours of development deep inside the embryo at a depth up to 80 µm, which is typically twice the scattering length of near infrared light in this embryo at this stage. These properties make mesoderm spreading challenging to image without compromising viability. Conventional confocal fluorescence microscopy is limited to a half of the required imaging depth (Figure 1C), and typically induces strong photo-toxicity. In order to circumvent these imaging limitations, 2-photon excited fluorescence (2PEF) microscopy appeared to be the most adapted technique. It still requires careful optimization of each imaging parameter, such as the fluorescent labeling, the mounting procedure, or the illumination and collection characteristics, in order to reach the image quality necessary to support computational analysis while at the same time maintaining embryo viability.

Embryos were aged for 3 hours at 25°C and dechorionated by hand. Heptane glue was used to cement embryos to a coverslip ventral side up and prevent any drift during the image acquisition. They were immersed in H_2O and placed directly above a large working distance, low magnification, high numerical aperture, and water-immersion objective (C-Aprochromat 40X/1.1 N.A. W Corr UV-VIS-IR, Carl Zeiss Inc.), preventing strong refractive index mismatch. The high numerical aperture and low magnification of the objective optimize the light collection when imaging deep inside the scattering embryo *(S1)*. Each embryo was imaged using 2PEF microscopy with a Zeiss LSM 510 inverted microscope (Carl Zeiss Inc.) at 940nm wavelength (Chameleon Ultra laser, Coherent Inc.). This high wavelength allows reduction of scattering, photo-toxicity and endogenous fluorescence signal from the yolk, while optimizing GFP excitation. $200x200x80\mu m^3$ 3D-stacks with $0.5x0.5x1\mu m^3$ voxel size and 1.9µs pixel dwell time were typically acquired every 45-50 seconds for approximately 3 hours. Viability was

scored by morphological changes of histone-labeled nuclei, timing of germband elongation, cell division delay, and ability to hatch to larvae. The fluorescence signal was collected in epi-collection using a 680 nm short pass filter, allowing collection of more fluorescent light than the standard 500-550nm filter for GFP. In order to increase the fluorescent signal-to-noise ratio when imaging in depth, forward emitted and scattered photons in the transmitted direction were back-reflected using a silver mirror positioned on the dorsal side of the embryo. A significant amount of these photons were epi-collected, with an increase of signal-to-noise reaching ~30%. This procedure was easier and more efficient than the use of a second detection in trans on the LSM 510 microscope. Mutant embryos were aged to stage 13 post-imaging and confirmed using a Dfd-GMR-YFP balancer. The *htl* mutation was recombined into a *klarschist* background (a lipid transport defective embryo) to clear the lipid-rich cells, thus decreasing the scattering properties of the tissue and increasing the imaging depth. *Klarschist* embryos (in the absence of the *htl* mutation) exhibit normal mesoderm migration (Figure S5 and S6).

3-D cell tracking

Imaris (Version 5.7, Bitplane Inc.) was used for all initial analysis of images. Stacks were rendered into 3D volumes. The fluorescent signal from the nuclei was segmented in 3D using the spot segmentation procedure of Imaris. Segmented nuclei were tracked through the time-sequence by applying the Imaris auto-regressive model for spot motion in 3D. Mesoderm and ectoderm tracks were first separated based on the fluorescent signal intensity, as the signal from ectoderm cells at the surface of the embryo appears stronger. This separation was then completed visually. Cell divisions were tracked manually by connecting separate tracks. The tracking data were manually corrected using the track editing function of Imaris. In addition, nuclear segmentation had to be completed semi-automatically for a significant number of mesoderm cells using the manual spot function in Imaris. The cell tracking procedure was helped with custom-made Imaris functions using ImarisXT and Matlab (The MathWorks Inc.) scripts. Typically 100 mesoderm cells

(see Figure S5) and ~1500 ectoderm cells were tracked for each embryo, corresponding to ~100,000 cell positions defined over time. All tracking analyses were performed using raw images. Sequences used for movies and figures were treated with a Gaussian filter applied to the entire image to improve image clarity. Overall, 3 wild-type embryos, 3 *htl* embryos (two in the *klar* background and one in the wild-type background), and 2 *klar* embryos were tracked and used for further analysis.

Cell tracking analysis

Cell tracking data were exported from Imaris to Matlab. Cell trajectories were analyzed with custom Matlab scripts. The gaps in cell tracks were filled with linear interpolation of cell positions.

Cylindrical coordinates

The main axis (**L**-axis) of the cylindrical coordinate system (**r**,**θ**,**L**) corresponds to the anterior-posterior axis of the embryo (Figure S1) and was defined by fitting a cylinder to the ectoderm cell positions at stage 7 of development. A least-squares cylinder was fitted to the cell positions using a Gauss-Newton algorithm. The spatial positions $\mathbf{r}_i(t)$, $\boldsymbol{\theta}_i(t)$, and $\mathbf{L}_i(t)$ of each cell *i* were subsequently computed using the cylindrical coordinates (see Fig S1). The **L**=0 position was defined arbitrarily along the **L**-axis (close to the cephalic furrow position, positive value towards the posterior direction), the **r**=0 position corresponds to the center of the embryo and the **θ**=0 position was defined as the position of the midline. The midline position was obtained experimentally by tracking 6 cells from the neuro-ectoderm over time. During the time of acquisition, the embryos usually exhibit some solid rotation around the anterior-posterior axis. This angular drift was corrected by subtracting the angular value of the midline position from the angular position of every cell. No significant translational drift of the embryos was observed during the time of acquisition. Defining cell positions in the cylindrical coordinate system allows for artificial unwrapping of the embryo. When the unwrapped cell positions are imported back into Imaris for display using ImarisXT (Movie S4), visualization of the

motions in this way facilitates a better understanding of the spreading movement. The main morphogenetic events of mesoderm formation and ectoderm germ-band elongation (*S2, S3*) are observed in specific directions of the cylindrical system. The radial direction, **r,** corresponds to a movement from the center to the outside of the embryo; mesoderm cells undergo furrow collapse and intercalation mainly in the **r** direction (Figure 2C). The angular direction, $\boldsymbol{\theta}$, depicts the medio-lateral movements of cells, such as spreading of the mesoderm and convergent movement of the ectoderm (Figure 2D). Finally, the anterior-posterior direction, **L**, corresponds to movement of cells along the length of the embryo, as occurs during germ-band elongation (Figure 2E).

Time synchronization and spatial color-codes

Wild-type and *htl* sequences were synchronized in time by defining t=0 minutes as the onset of ectoderm cell movement in the anterior-posterior direction (L-axis), corresponding to the onset germband elongation. Stages 7, 8, 9 and 10 of development correspond to the time windows: $\mathbf{t}$<0min, 0min<$\mathbf{t}$<30min, 30min<$\mathbf{t}$<70min, and $\mathbf{t}$>70min, respectively. The upper and lower furrow cells were defined for $\mathbf{r}_i$(stage 7) < $0.6R_0$ and $\mathbf{r}_i$(stage 7) > $0.6R_0$, respectively, with R_0 being the radius of the fitted cylinder (typically representing the radius of the embryo) and $\mathbf{r}_i$(stage 7) the radial position of each cell *i* during stage 7. The radial and angular color codes were also defined depending on the distribution of $\mathbf{r}_i$ and $\boldsymbol{\theta}_i$ values, respectively, within the mesoderm furrow at stage 7. After each cell division, the color code describing upper/furrow origins for the two daughter cells was defined as that of the originating mother cell. The color code used in Figure 4H and 4I corresponds to [$0.35\ R_0$;$0.9\ R_0$] at the end of the spreading process.

Cell division and cell intercalation

A cell division event was defined as the time point when cell tracks split into two different tracks and was identified computationally. Cell division orientation was computed automatically as the orientation of the vector joining the two daughter cells (**u** vector in Figure S7A) at the time point immediately following the division. The

normalized **u** vectors for each cell division are displayed in 3D in Figure S7A. Cell intercalation events were automatically identified from the tracking data using a custom MatLab script by analyzing the relative movement in the radial direction between each mesoderm cell and its nearest neighbors over a 30 minute time window.

Customized statistical analyses

Custom designed statistical analyses were created in order to analysis large amounts tracking data for the purpose of decomposing movements and to provide a measure of consistency of mesoderm cell spreading between embryos.

Ectoderm/Mesoderm correlation analysis and ectoderm movement subtraction

For the velocity correlation analysis (Figure 2F-H and Fig S4), the instantaneous velocity of each cell was computed. Before that, the cell trajectories were smoothed in time using a 5-point Loess quadratic fit applied to each spatial component. The instantaneous velocity was estimated using low time sampling (a measurement every 13 minutes) by dividing the cell displacement by the time delay; this time sampling was most appropriate for analysis of movement in the 3 directions **r**, **θ**, and **L**, as in the **r** and **θ** directions the movement is slow (~0.5 μm/min) relative to the movement in **L**. However, using a time sampling of 13 minutes, the distribution of values along the **L** axis is discontinuous (refer to Figure 2H) due to the rapid movement along this axis (up to 5 μm/min) during germ-band elongation (GBE), followed by little movement upon completion of GBE (refer to Figure 2E). If a smaller time sampling is used, then the correlation is continuous. Each spatial component (v_r, v_θ, v_L) of mesoderm cell velocity was plotted depending on the average spatial components of the 6 nearest ectoderm cell neighbors. The correlation coefficient refers to the Pearson product-moment correlation coefficient.

To subtract the movement of the ectoderm from the mesoderm cells over time, the average displacement ($\Delta\mathbf{r}$, $\Delta\boldsymbol{\theta}$, $\Delta\mathbf{L}$) of six neighboring ectoderm cells was removed from the displacement of each mesoderm cell between each time point. The new mesoderm

cell positions were subsequently imported back into Imaris for display using ImarisXT (Figure 2I, Figure S3, and Movie S5).

The correlation analysis of mesoderm and ectoderm cell movements is a demonstration of the strong mechanical coupling of these two movements in the **L** direction (Figure 2). This quantitative demonstration identified particular mesoderm cell movements that exhibit no coupling with ectoderm movements. We, therefore, limited our analysis of mesoderm cell movements to two dimensions (**r** and **θ** axes), the directions in which no coupling between mesoderm and ectoderm cell movements was observed. In this way, we were able to simplify the study of wild-type and mutant phenotypes.

Consistency analysis of mesoderm cell spreading

In order to compare one embryo to the other as well as to compare wild-type and mutant phenotypes, we developed a statistical analysis to study the overall pattern of cell spreading. The angular positions of each cell at the onset ($\boldsymbol{\theta}_{start}$) and at the end ($\boldsymbol{\theta}_{end}$) (Figures S4A and B) of the spreading process are obtained from the tracking data. These normalized values are plotted in a single 2D-graph (Figure S4C). The spatial organization of the spreading observed in wild-type embryos (Figure 3A) is translated into a regular distribution of points in the $\boldsymbol{\theta}_{end}(\boldsymbol{\theta}_{start})$ graph, which tends to align along a line, as shown in Figure S4C. For clarity purpose, the color code used for each cell in Figure 3A and S4B is kept the same in Figure S4C. This distribution is characterized by fitting a regression line: $\boldsymbol{\theta}_{end} = A.\boldsymbol{\theta}_{start} + B$. The variables A and B are estimated using a least-squares method, and the resulting correlation coefficient is R.

A, B and R have specific biological meanings. B is close to 0 when the spreading is symmetrical with respect to the midline. The slope A of the line characterizes the general spreading behavior and its strength. Values of A=1 and B=0 describe the case in which no movement has occurred at all. Values of A>1 describe normal spreading (white area in Figure S4C-K); the higher the value, the stronger the spreading is. A≤1 means an

absence of movement or abnormal movement has occurred (grey area in Figures S4C and S4E-K). For clarity purpose, the graphs S4D-E show three typical cases (assuming that B=0). If a cell is spreading normally (blue line in S4D), the $\theta_{end}(\theta_{start})$ position of the cell is in the white area (blue cross in S4E, with A>1). If A>0 and <1 (red color in S4E), the cell is moving toward the midline (red line in S4D). If A<0 (green color in S4E), the cell is crossing the midline and migrating to the opposite side of the embryo (red line in S4D).

*Note :*The term coupled is used when a quantitative parameter (such as the velocity) in a specific population of cells (mesoderm) is correlated to the same parameter in another population (ectoderm). This correlation is estimated using a Pearson product-moment correlation coefficient.

The term collective is used when a specific behavior (such as the spreading angle relation $\theta_{end}(\theta_{start})$) is quantitatively defined and shared by every cells of a single population. The collective nature of the process is quantified by applying a regression model and estimating the resulting correlation coefficient (R in this study). When the R value is close to 1, the quantitative behavior following the model is claimed to be collective.

II. Supplemental Figures

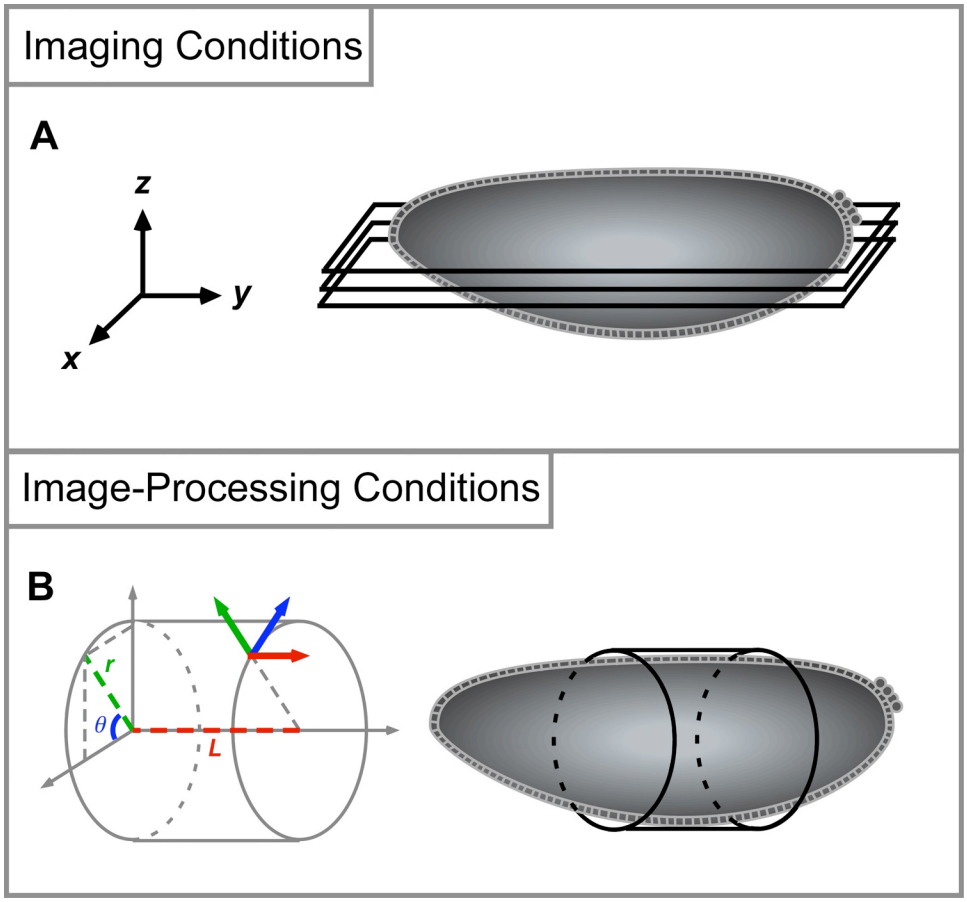

Figure S1. Coordinate systems used during imaging and analysis processes. (A) Stacks of two-photon images are collected using traditional Cartesian coordinates (**x,y,z**). This system works well for imaging in 3D space and is employed in most microscope setups. Initial tracking data created with Imaris also uses this coordinate system. (B) During image processing, we change to a cylindrical coordinate system (**r,θ,L**) to conform roughly to the body plan of the embryo, which makes analysis of each morphogenetic movement along each axis more straightforward. **r** corresponds to the radial position of each cell over time (e.g. furrow collapse, intercalation). The 0 value of **r** defines the center of the embryo. **θ** represents the angular movement of cells (spreading). The 0 value of **θ** is determined experimentally as the position of the

embryonic ventral midline (see Materials & Methods for additional information). **L** corresponds to the location of cells along the anterior-posterior axis (germband elongation).

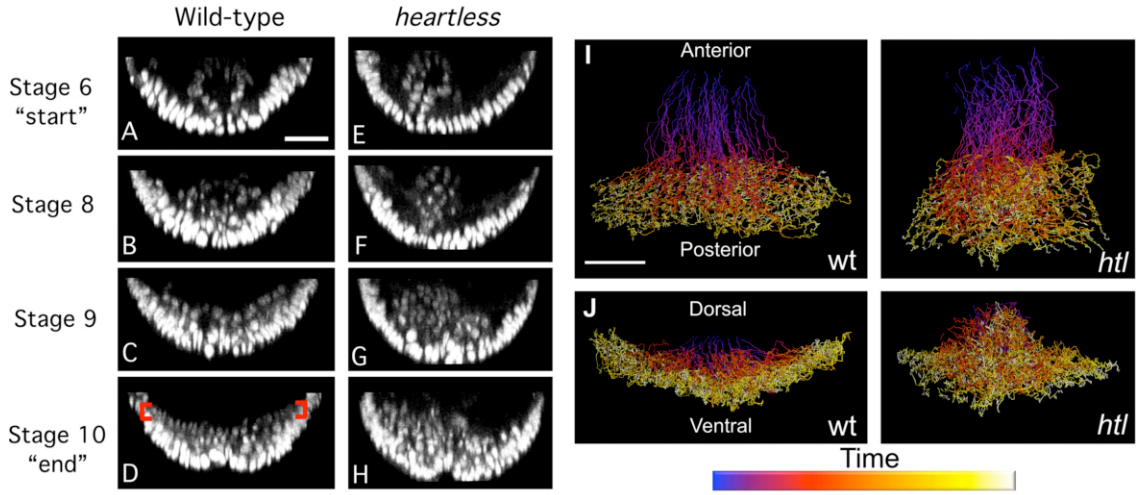

Figure S2. Virtual cross-sections and tracking data for H2A-GFP embryos in wild-type and *htl* backgrounds. (A-H) 5 μm thick cross-sections through H2A-GFP data were created using Imaris software. Mesoderm cells can be observed inside of the embryo at each stage, and each main morphogenetic event is represented: furrow formation (stage 6; A,E), the collapse of the furrow (stage 8; B,F), spreading (stage 9; C,G), and formation of the monolayer (stage 10; D,H, red brackets). *htl* mutant embryos, also expressing H2A-GFP, show defects in mesoderm spreading similar to those documented in the literature. Nuclei were tracked over time using Imaris. (I) Dorsal view of tracking data in wild-type and *htl* embryos. (J) Posterior view of tracks from wild-type and *htl* embryos. Time is represented by color (purple=early, yellow=late). Scale bar = 20 μm.

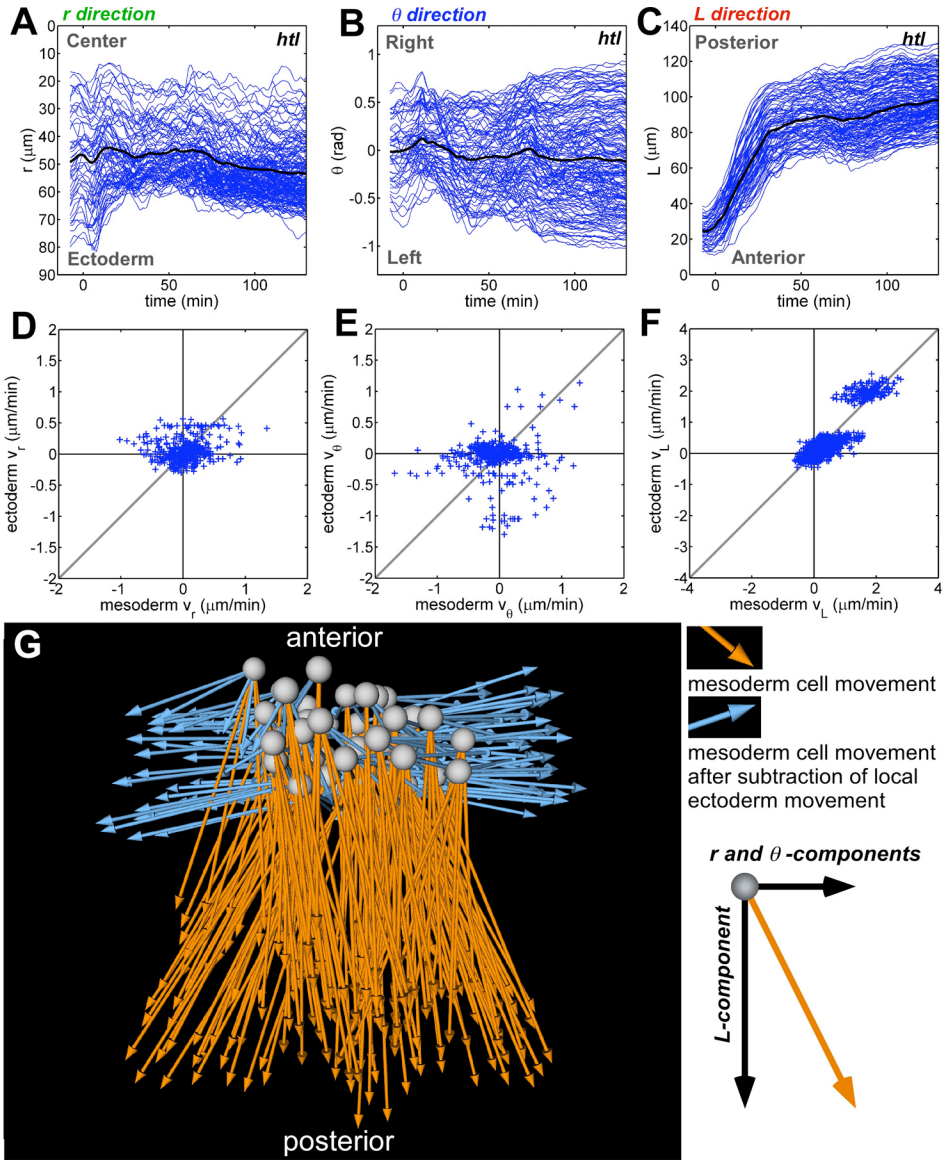

Figure S3. Decomposition of movement, correlation data and ectoderm subtraction for *htl.* Cylindrical coordinates are used to position cells according to the body plan of embryo at stage 6. Each axis of the cylinder corresponds to a specific morphogenetic movement: (A) **r** corresponds to the radial position of each cell over time (e.g. furrow collapse, intercalation) The 0 value of **r** defines the center of the embryo. (B) **θ**

represents the angular movement of cells (spreading). The 0 value of **θ** is determined experimentally as the position of the embryonic ventral midline. (C) **L** corresponds to the location of cells along the anterior-posterior axis (germband elongation). Each blue line represents the movement of one cell in time. (D-F) Statistical analysis of correlation of the velocity of mesoderm and ectoderm cells along the (D) radial, (E) angular, and (F) AP axes in a *htl* mutant, with correlation values of 0.24 +/- 0.21, 0.13 +/- 0.12, and 0.86 +/- 0.06, respectively. (G) Displacement of the mesoderm before (orange) and after (blue) subtraction of local ectoderm movement in a *htl* mutant.

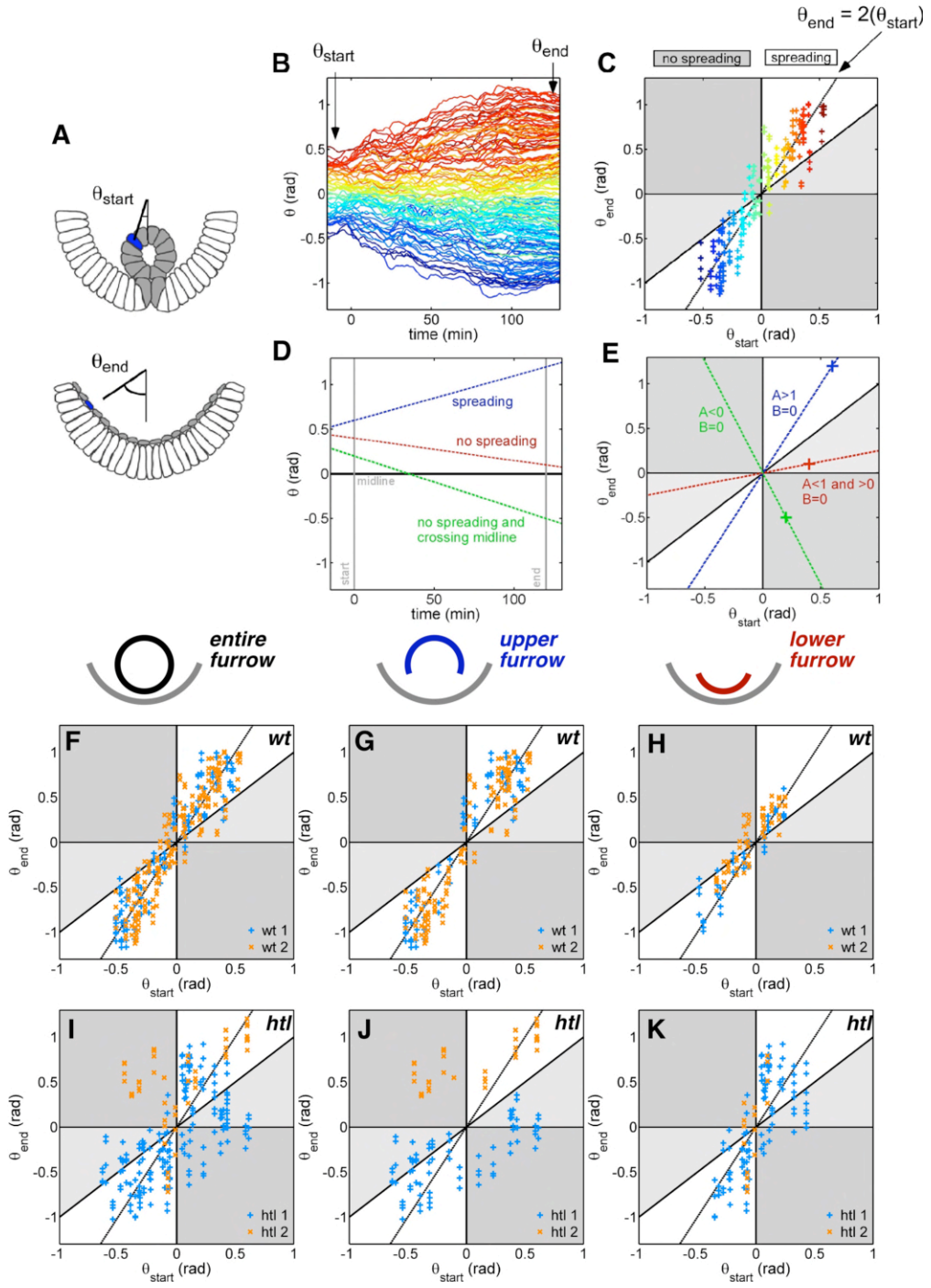

Figure S4. Spreading consistency analysis: $\theta_{start}(\theta_{end})$ graphs. (A-C) The mesoderm spreading is analyzed by obtaining the angular position of each cell at the onset and the

end of the process, θ_{start} and θ_{end}, respectively (A). The color code is similar to Figure 3A. The spatial organization observed in a θ(time) graph (B, similar to Figure 3A) is translated into a 2D-graph where the $\theta_{end}(\theta_{start})$ position of each cell is plotted (C). This graph is used to characterize the spreading by fitting a regression line [$\theta_{end} = (A.\theta_{start}) + B$] on the experimental data. Data points that fall within the white region of the graph represent spreading cells, while points in grey regions represent cells that do not spread with the collective. The values of A and B are estimated using a least-squares method, and the correlation coefficient R of the fitting is displayed in the table of Figure S6 for different embryos. (D-E) θ(time) graph (D) and $\theta_{end}(\theta_{start})$ graph (E) for three typical cell movements assuming B=0: normal spreading (blue color, A>1 and B=0 line in E), movement towards the midline (no spreading, red color, A<1 and >0 and B=0 line in E), and movement towards the opposite side of the embryo (no spreading and crossing the midline, green color, A<0 and B=0 line in E). (F-H) Wild-type embryo spreading profile within the entire mesoderm (F), upper furrow (G), and lower furrow (H). The orange or blue ticks represent datapoints for each of two embryos of either *wt* or *htl* backgrounds. (I-K) *htl* embryo spreading profile in the entire mesoderm (I), upper (J) and lower furrow (K). Cells in the lower furrow of *htl* embryos display wild-type behavior (compare to H) ; whereas cells in the upper furrow fall into two categories. Most spread abnormally (grey area), but some spread normally (white area).

A

Embryos	Cell population	A	± ΔA	B	± ΔB	R
wt 1	all (126)	1.85	0.12	0.03	0.04	0.94
wt 2	all (186)	1.93	0.12	0.01	0.03	0.92
wt 3	all (90)	2.36	0.25	-0.02	0.05	0.90
wt 4 (klar)	all (138)	1.98	0.14	0.05	0.04	0.92
wt 5 (klar)	all (56)	2.01	0.22	0.03	0.07	0.93
all wt embryos	***all (596)***	***1.96***	***0.06***	***0.03***	***0.02***	***0.93***
htl 1	all (185)	0.92	0.18	-0.11	0.06	0.61
htl 2	all (53)	0.69	0.33	0.48	0.12	0.51
htl 3	all (46)	1.34	0.29	-0.21	0.09	0.81
all htl embryos	***all (284)***	***0.98***	***0.16***	***-0.02***	***0.05***	***0.58***
wt 1	upper furrow (82)	1.90	0.15	0.04	0.05	0.94
wt 2	upper furrow (128)	1.99	0.13	-0.04	0.04	0.93
wt 3	upper furrow (36)	2.69	0.49	0.02	0.10	0.89
wt 4 (klar)	upper furrow (77)	2.08	0.17	0.10	0.06	0.94
wt 5 (klar)	upper furrow (36)	1.96	0.26	0.07	0.10	0.94
all wt embryos	***upper furrow (359)***	***2.02***	***0.08***	***0.04***	***0.03***	***0.93***
htl 1 (klar)	upper furrow (81)	0.54	0.13	-0.29	0.05	0.69
htl 2 (klar)	upper furrow (37)	0.51	0.13	0.69	0.06	0.79
htl 3	upper furrow (28)	1.16	0.23	-0.34	0.08	0.90
all htl embryos	***upper furrow (146)***	***0.78***	***0.19***	***-0.05***	***0.08***	***0.55***
wt 1	lower furrow (44)	1.63	0.20	-0.01	0.05	0.93
wt 2	lower furrow (58)	1.58	0.22	0.10	0.04	0.89
wt 3	lower furrow (54)	2.13	0.24	-0.05	0.05	0.93
wt 4 (klar)	lower furrow (61)	1.65	0.21	-0.01	0.05	0.89
wt 5 (klar)	lower furrow (20)	2.37	0.56	-0.03	0.10	0.90
all wt embryos	***lower furrow (237)***	***1.74***	***0.11***	***0.01***	***0.02***	***0.90***
htl 1 (klar)	lower furrow (104)	1.79	0.34	-0.01	0.07	0.71
htl 2 (klar)	lower furrow (16)	4.14	2.42	0.10	0.19	0.70
htl 3	lower furrow (18)	1.98	0.84	-0.07	0.16	0.78
all htl embryos	***lower furrow (138)***	***1.83***	***0.31***	***-0.01***	***0.06***	***0.71***
htl 1 (klar)	far from ectoderm (83)	0.45	0.17	-0.15	0.06	0.52
htl 2 (klar)	far from ectoderm (33)	0.43	0.36	0.54	0.12	0.40
htl 3	far from ectoderm (38)	1.09	0.34	-0.14	0.10	0.73
all htl embryos	***far from ectoderm (154)***	***0.39***	***0.19***	***0.02***	***0.07***	***0.31***
htl 1 (klar)	close to ectoderm (102)	1.90	0.27	0.06	0.07	0.81
htl 2 (klar)	close to ectoderm (20)	2.04	0.61	-0.02	0.23	0.86
htl 3	close to ectoderm (8)	1.85	0.75	-0.28	0.25	0.93
all htl embryos	***close to ectoderm (130)***	***1.93***	***0.21***	***0.03***	***0.06***	***0.85***

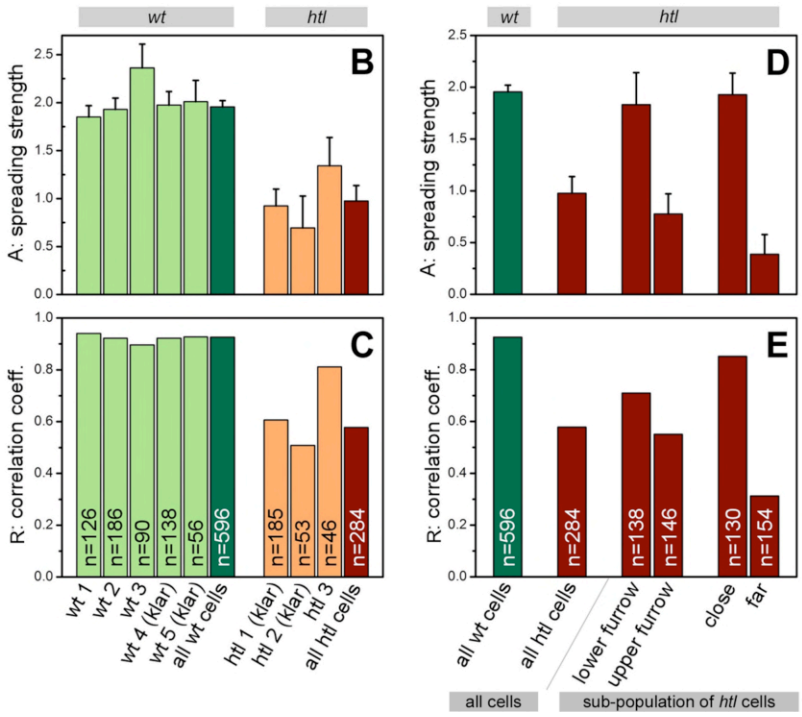

Figure S5. Spreading consistency analysis: table of linear regression and main conclusions. (A) The $\theta_{end}(\theta_{start})$ graphs (e.g. Figure S4C) are analyzed by fitting a

regression line ($\theta_{end} = A.\theta_{start} + B$) on the experimental data. The estimated A and B values (with a 95% confidence interval), as well as the resulting correlation coefficient R are indicated in this table for different cell populations. The number of cells analyzed in each case is indicated between brackets. (C-E) "A" (C) and "R" (D) values of five *wt* embryos (including the data of two *klar*, which for all extent of purposes shares a similar phenotype with *wt*) versus three *htl* embryos are indicated in light green and light red, respectively. The same analysis performed by pooling the cells from all *wt* or *htl* embryos are plotted in dark green and dark red, respectively. (E and F) The analysis (A and R values) of two *htl* cell populations are performed using either the upper/ lower furrow cutoff (middle of the graphs) or the close / far position from the ectoderm at the end of the process (right of the graphs). When segregated, the *htl* cells coming from the lower furrow exhibited movements that were collective (i.e. higher A and R values), similar to *wt* cells; in contrast, the *htl* cells from the upper furrow displayed less coordination (i.e. low values for A and R). **n** indicates the number of cells used for the analyses. See Methods section for full description of approach.

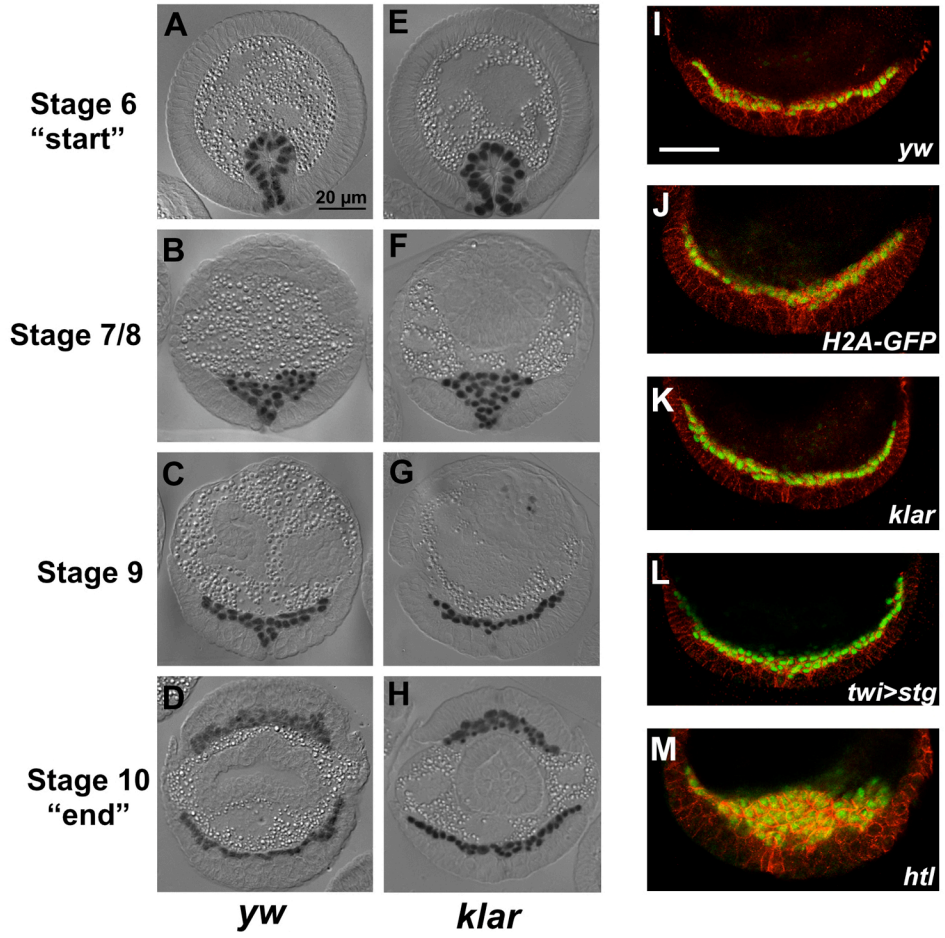

Figure S6. Wild-type and *klarschist* embryos show similar morphology in fixed sections. (A-D) *yw* ("wild-type") and (E-H) *klar* (*klarschist*) embryos were stained with an anti-Twist antibody and sectioned. (A and E) Stage 6, (B and F) Stage 7/8, (C and G) Stage 9, and (D and H) Stage 10 sections are shown. (I-M) Fluorescent sections of embryos with anti-Twist (green) and anti-Neurotactin (red) antibodies show morphology of different genetic backgrounds. *yw* (I), ubiquitous H2A-GFP (J), *klarschist* (K), and embryos ectopically expressing string in the mesoderm (twi-Gal4 UAS-string) (L) embryos all show wild-type mesoderm morphology (see "yw"). *htl*^{AB42} embryos (M) have a multi-layered mesoderm, indicative of defective mesoderm migration.

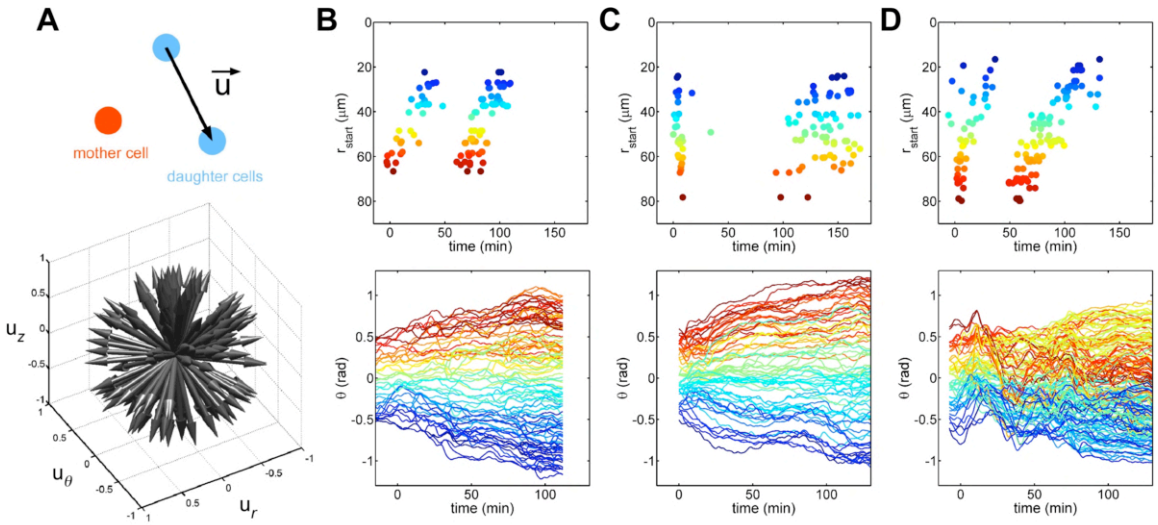

Figure S7. Disrupting the spatial or temporal patterns of division in the mesoderm does not affect the spreading pattern. (A) Cell division orientation in wild-type embryos is random (N=8 embryos). Each arrow shows the division orientation, **u**, of the daughter cells for one particular mother cell, see diagram at the top for example. (B) Wild-type pattern of divisions and spreading correlate with radial position, as cells closer to the ectoderm divide first followed by cells farther away. See Figure 4 and Figure S5 for color code. (C) *klarschist* embryos with mild induced photoxicity exhibit abnormal division patterns consistent with previous studies of photoxicity. The spreading pattern is not affected by this disruption. (D) *htl* mutants display wild-type division patterns. The spreading pattern, however, is highly disrupted.

III. Movie Legends

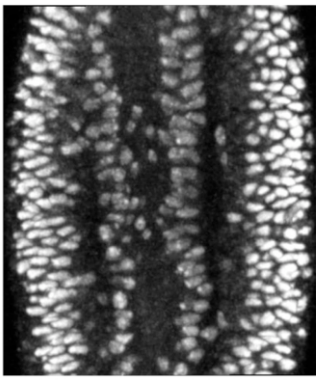

Movie 1. Two-photon excitation of ubiquitous H2A-GFP in early embryos. Images of a H2A-GFP expressing embryo taken from dorsal view (10 μm thick stack 50 μm deep into the embryo) or a posterior view (5 μm thick stack) using two-photon microscopy. Scale bar = 20 μm**.**

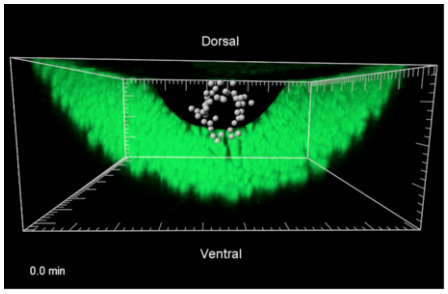

Movie 2. **Segmentation and tracking of mesoderm nuclei in wild-type embryos using Imaris software.** Spots represent mesoderm nuclei tracked over time (see Materials and Methods for more details). Ectoderm H2A-GFP raw data is kept in for reference. Tracks are represented by lines with a temporal color code, where purple represents early time points and yellow represents late time points (see scale bar in Figure 1). The first view is dorsal, and the second view is posterior. Large grid mark = 20 μm.

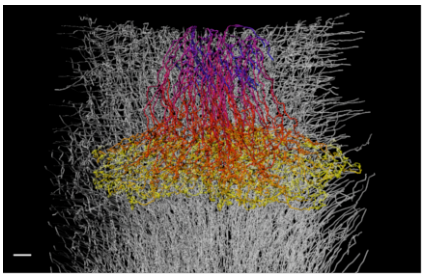

Movie 3. **3D tracks of mesoderm and ectoderm cells over time.** A dorsal view of mesoderm tracks is first shown in with a temporal color scale (see Figure 1) on top of grey ectoderm tracks. Displacement vectors for mesoderm and ectoderm are represented by orange and grey arrows, respectively. Scale bar = 20 μm.

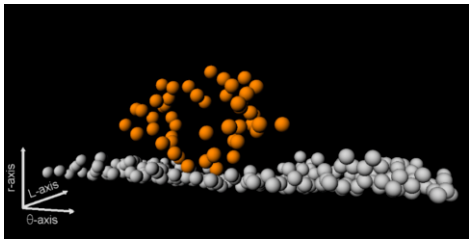

Movie 4. Visualization of cylindrical coordinate system. Data from each embryo can be unwrapped according to cylindrical coordinates (See Figure S1 and Materials & Methods for more details).

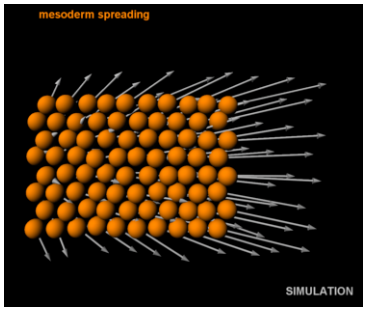

Movie 5. Ectoderm Subtraction in a wild-type embryo (simulation). The local movement of ectoderm cells is subtracted from the mesoderm to show autonomous movement of the mesoderm (see Materials & Methods for more details).

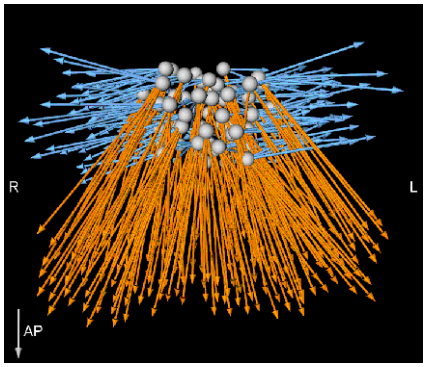

Movie 6. Ectoderm Subtraction in a wild-type embryo (experimental data). Displacement of the mesoderm before (orange) and after (blue) subtraction of local ectoderm movement (3-D version of Figure 2I, see Materials & Methods for more details). A= Anterior, P=Posterior, L=Left, R=Right, D=Dorsal, V=Ventral.

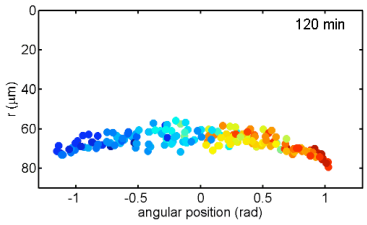

Movie 7. Wild-type cell movements along radial and angular axes (theta color code). The position of each cell is represented with a dot. Its color encodes for the angular position at the onset of mesoderm collapse (stage 7). In addition, dots representing dividing cells are circled with a black line at the time of the division.

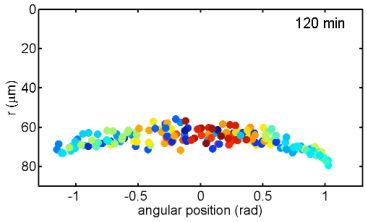

Movie 8. Wild-type cell movements along radial and angular axes (radial color code). The position of each cell is represented with a dot. Its color encodes for the radial position at the onset of mesoderm collapse (stage 7). In addition, dots representing dividing cells are circled with a black line at the time of the division.

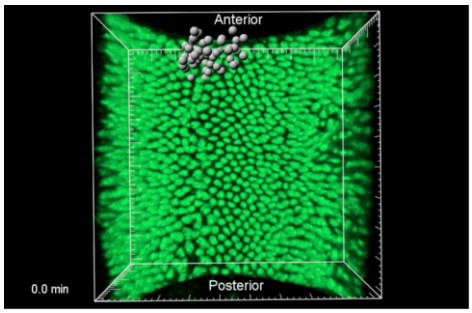

Movie 9. Segmentation and tracking of mesoderm nuclei in *htl* mutant. Mesoderm nuclei are represented by spots, with raw ectoderm H2A-GFP data underneath. Tracks have a temporal color code (see scale bar in Figure 1). The first view is dorsal, and the second view is posterior. Large grid mark = 20 μm

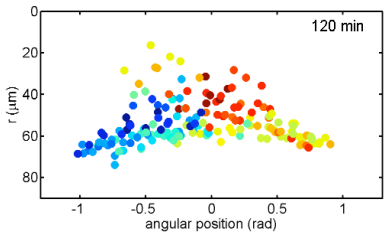

Movie 10. *htl* cell movements along radial and angular axes (angular color code). The position of each cell is represented with a dot. Its color encodes for the angular position at the onset of mesoderm collapse (stage 7). The dots of dividing cells are circled with a black line.

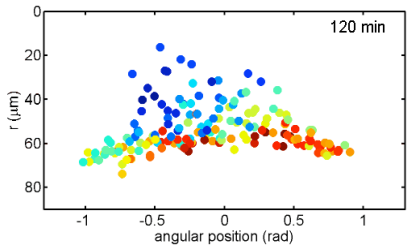

Movie 11. *htl* cell movements along radial and angular axes (radial color code). The position of each cell is represented with a dot. Its color encodes for the radial position at the onset of mesoderm collapse (stage 7). The dots of dividing cells are circled with a black line.

IV. References

S1. E. Beaurepaire, J. Mertz, *Appl Opt* **41**, 5376 (Sep 1, 2002).

S2. K. D. Irvine, E. Wieschaus, *Development (Cambridge, England)* **120**, 827 (Apr, 1994).

S3. J. A. Zallen, J. T. Blankenship, *Semin Cell Dev Biol* **19**, 263 (Jun, 2008).